

Sulfate attack monitored by microCT and EDXRD: Influence of cement type, water-to-cement ratio, and aggregate

N.N. Naik^a, A.C. Jupe^a, S.R. Stock^b, A.P. Wilkinson^c, P.L. Lee^d, K.E. Kurtis^{a,*}

^a*School of Civil and Environmental Engineering, Georgia Institute of Technology, Atlanta, Georgia, United States*

^b*Institute for Bioengineering and Nanoscience in Advanced Medicine, Northwestern University, Chicago, Illinois, United States*

^c*School of Chemistry and Biochemistry, Georgia Institute of Technology, Atlanta, Georgia, United States*

^d*Advanced Photon Source, Argonne National Laboratory, Argonne, Illinois, United States*

Received 28 May 2005; accepted 7 June 2005

Abstract

X-ray microtomography (microCT) and spatially resolved energy dispersive X-ray diffraction (EDXRD) were used in combination to non-destructively monitor the physical and chemical manifestations of damage in Portland cement paste samples subjected to severe sodium sulfate attack. Additional measurements of expansion and compressive strength were made on complementary mortar and cement paste specimens. Specifically, the influences of cement type (ASTM Types I and V), water-to-cement ratio (0.485 and 0.435), and the presence of aggregate on the rate and forms of damage were examined. As expected, Type V cement samples exhibited less cracking and expansion than the Type I cement samples. EDXRD indicated an anticorrelation between ettringite and gypsum in the near-surface region for Type V samples, which may be associated with crack formation. An unanticipated result for Type I cement pastes was that cracking was apparent at earlier exposure times and progressed more rapidly for samples with w/c of 0.435, than for those with w/c of 0.485. Possible mechanisms for this behavior are proposed. The presence of aggregate particles resulted in a more rapid rate of cracking, as compared to the corresponding cement paste sample.

© 2005 Elsevier Ltd. All rights reserved.

Keywords: Concrete; Diffraction; Durability; Gypsum; Ettringite; Expansion; Tomography; X-ray

1. Introduction

The resistance of Portland cement concrete to external sulfate attack is governed by many parameters related to materials selection and mixture proportioning. These include cement composition, water-to-cement ratio (w/c), use and proportion of supplementary cementing materials, characteristics of the aggregate (e.g., maximum size), and the use of chemical admixtures, among others. w/c and cement composition, in particular, are two key factors affecting the sulfate resistance of concrete mixtures [1–4]. Also, the addition of aggregate is well known to lead to increased permeability in concrete as compared to cement

paste. As each of these three parameters can be controlled during the design of the concrete mixture, the influence of cement type, w/c , and the presence of aggregate are of particular interest in understanding the progress of sulfate attack.

However, considerable uncertainty remains in optimally selecting and proportioning materials for sulfate resistance in concrete [5–8]. For the most sensitive and critical of applications – hazardous waste containment vessels containing sulfate-rich materials or buried in sulfate-containing soils – these deficiencies become safety issues. For more typical applications, such as hydraulic structures or housing, these deficiencies are economic and environmental sustainability issues.

Thus, for both critical and typical applications where sulfate exposure is expected, laboratory testing may be warranted to characterize the sulfate resistance of potential

* Corresponding author. 790 Atlantic Dr., Atlanta, GA 30332-0355, United States. Tel.: +1 404 385 0825; fax: +1 404 894 0211.

E-mail address: kkurtis@ce.gatech.edu (K.E. Kurtis).

material combinations. The most common accelerated test for assessing sulfate resistance relies upon measurements of expansion [9]. Other tests monitor changes in strength with sulfate exposure [10,11].

While such measures produce data important for assessing relative performance under particular conditions, it is difficult to extract a more mechanistic understanding of the progress of sulfate attack in a sample with particular characteristics or in a particular environment. That is, the measured response (i.e., expansion, loss in strength) does not reveal the specific changes occurring in the sample (e.g., internal or external cracking, spalling, and compositional changes). Two emerging X-ray characterization methods – X-ray microtomography (microCT) and energy dispersive X-ray diffraction (EDXRD) – can add insight into the progression of sulfate induced-damage in cement-based materials.

The goal of this research was to characterize the influence of some “internal” parameters (i.e., those related to materials selection and mixture proportioning) on the progression of sodium sulfate attack. Specifically, an integrated approach assessed the effects of w/c , ASTM cement type, and the presence of aggregate; this included non-destructive monitoring of physical changes using microCT and of changes in constituent phases using EDXRD. Observations were made on cement paste and cement paste-aggregate samples with continued exposure to a sodium sulfate solution with 10,000 ppm sulfate, which corresponds to severe conditions defined by the American Concrete Institute’s (ACI) Committee 201: Durability of Concrete [12] or the lower limit for Class 3 exposure in that committee’s more recent definitions [13]. In addition, complementary measurements were made of expansion and strength change with duration of exposure. Comparing data describing physical and chemical changes in microstructure, expansion, and changes in strength with sulfate exposure produced results that both corroborate and dispute the current understanding of sulfate attack in Portland cement-based materials.

2. Experiment details

2.1. Materials and sample preparation

For characterization by both microCT and EDXRD, cylindrical cement paste samples approximately 4 cm long and 1.2 cm in diameter were cast in plastic vials from mixtures of ASTM Type I or Type V cement and de-ionized water (resistivity of 18.2 M Ω cm). Oxide analysis and Bogue potential composition for the ASTM Type I cement, obtained from Holcim (US) Inc., and the Type V cement, obtained from TXI Riverside Cement, are shown in Table 1. Pastes were prepared at w/c of 0.485 and 0.435. The higher w/c (0.485) was selected to conform with ASTM C1012, which is a standard test method for length change of

Table 1

Chemical analyses of ASTM Type I and Type V Portland cements and corresponding Bogue potential compositions

Oxide/phase	Type I (wt.%)	Type V (wt.%)
SiO ₂	19.84	22.30
Al ₂ O ₃	5.44	3.55
Fe ₂ O ₃	2.69	3.65
CaO	65.57	63.46
MgO	0.65	0.32
Na ₂ O	0.14	0.17
K ₂ O	0.33	0.37
Total alkalis as Na ₂ O	0.36	0.41
TiO ₂	0.48	0.15
Mn ₂ O ₃	0.02	0.32
P ₂ O ₅	0.25	0.20
SrO	0.21	0.04
BaO	0.01	0.00
SO ₃	3.03	2.99
LOI	1.33	1.49
Insoluble residue	0.20	0.24
C ₃ S	67.2	53.3
C ₃ A	9.9	3.3
C ₂ S	6.2	23.8
C ₄ AF	8.2	11.1

hydraulic-cement mortars exposed to a sulfate solution. The lower w/c (0.435) was selected to provide measurements both above (i.e., 0.485) and below (i.e., 0.435) the maximum w/c of 0.45 recommended by ACI 201 [12] for severe sulfate exposure.

To investigate the effect of aggregate on sulfate damage, some samples were prepared with aggregate particles at an aggregate-to-cement ratio (agg/c) of 0.20 by mass. The aggregate was formed by crushing 0.5-mm thick, quartz single crystal wafers, which were surplus World War II materials. This material was used to provide good contrast between the cement paste and the aggregate when imaging by microCT. Particles passing the No. 30 sieve (0.6 mm) were rejected, giving the gradation in Table 2.

The aggregate volume in concrete is typically much greater than what was considered for the experiments. Such a high aggregate volume proportion results in much of the cement paste in a concrete residing in interfacial transition zones between the aggregate and paste. The properties of the transition zone, such as porosity and morphology of hydration products, are different from those of corresponding neat cement paste. In the current program it was possible to examine one value of aggregate proportion due to restrictions on time and resources. A low aggregate volume was selected to allow examination of the influence of the presence of aggregates, while avoiding issues with particle packing and edge effects which can occur in such a small sample volume and while retaining some paste volume which would be considered to be “bulk” (i.e., not transition zone).

As mix volumes were small, mixing of these cement paste and cement paste with aggregate samples for microCT and EDXRD was done by hand in a temperature-controlled laboratory at 22 ± 2 °C. Details of the mixture proportioning for these samples are shown in Table 3.

Table 2

Sieve analysis for the aggregate used to prepare samples for microtomography

Sieve	Size (mm)	Weight retained (%)	Cumulative retained (%)	Amount passing (%)
No. 4	4.76	0	0	100
No. 8	2.38	2.39	2.39	97.61
No. 16	1.168	70.42	72.81	27.19
No. 30	0.595	27.19	100	0

The procedure for measuring the effects of sulfate attack on compressive strength is based upon the sulfate resistance test method described by Mehta [10] and more recently implemented by Kurtis et al. [11]. Half-inch (1.27 cm) cement paste cubes were cast from the same two cements with w/c of 0.485 (Table 3), and the mixing procedure was the same as for the cylindrical samples used for microCT and EDXRD measurements. Compressive strength measurements were performed using a 22,000 lb. (9980 kg)-capacity, screw driven universal test machine with a load rate of 600 lb/min (272 kg/min). Compressive strength measurements were made on six replicate samples for each condition after 2, 4, 8, 17 and 24 weeks of exposure. Beyond 24 weeks exposure, samples were too damaged for continued compression testing.

For measurements of length change, mortar bar samples were cast in $1 \times 1 \times 11$ in ($2.5 \times 2.5 \times 28.5$ cm) brass molds from the same two cements, with w/c of 0.485 and 0.435 and sand-to-cement ratio (sand/ c) of 2.75 by mass (Table 3). The natural sand (FM=1.8) used was obtained from Brown Brothers quarry in Junction City, Georgia. The samples were mixed and cast in accordance with ASTM C 1012. Mixing of the mortar bars was done using a 5-L capacity Hobart mixer at 120 rpm. Six replicates were prepared for each mix (Table 3). Length change measurements were conducted weekly until 52 weeks of exposure. Average values were calculated from measurements generally of six replicates, but not on fewer than three replicate samples (as some samples failed during exposure).

All samples (i.e., Portland cement-based cylinders, cement paste cubes and mortar bars) were demolded after one day and were subsequently cured for two additional days in limewater at room temperature. The three-day curing period was determined as described in ASTM C

1012 [9], where the curing period is determined by the time necessary for the compressive strength of 2 in (5.08 cm) mortar cubes to reach 3000 psi (20.7 MPa). After curing, samples of each type were placed in sodium sulfate solutions, as described in Section 2.2. Some samples of each type were also stored in sealed containers at room temperature after the initial curing, to serve as controls.

2.2. Sulfate exposure condition

Sulfate solutions were prepared from reagent grade anhydrous sodium sulfate (obtained from Fisher Chemicals) and de-ionized water to give a sulfate ion concentration of 10,000 ppm. Samples were stored in sealed polypropylene containers at room temperature. The ratio of solution volume to sample surface area was kept constant at $2.4 \text{ cm}^3/\text{cm}^2$, which for the mortar bars corresponds to the solution-to-sample volume ratio of 4, as specified in ASTM C 1012 [9]. While ASTM C 1012 specifies that the frequency of replacement of sulfate solution coincide with measurements of length (which are on a weekly basis until 4 weeks and staggered henceforth), solutions were replaced weekly.

2.3. MicroCT

Details on the working principles of microtomography can be found in Refs. [14,15]. MicroCT was performed using a Scanco μCT 40 benchtop system with a 70 kVp X-ray tube. Data collection and processing was done with the aid of Scanco μCT 40 software. A detector with 2048×64 elements and $24\text{-}\mu\text{m}$ pitch was used. For most measurements, the experimental configuration was as follows: number of projections=390, integration time=350 ms, voxel size= $37 \mu\text{m}$ on edge. MicroCT was performed on the top half (i.e., from the free surface at casting to approximately 2 cm along the length of the cylinder) of the samples at 0, 4, 9/10, 12/13, 16/17, 21, 32/33, 36, 42, 52/53, and 78 weeks exposure time to monitor the progression of physical changes in the samples with increasing exposure time.

2.4. EDXRD

Spatially-resolved EDXRD measurements were made at Beamline 1-ID of the Advanced Photon Source (APS), a

Table 3

Mixture proportions

Parameter examined	Microstructural characterization			Compressive strength		Length change		
	Cement	w/c	Agg/ c	Cement	w/c	Cement	w/c	Sand/ c
Reference samples	I	0.485	–	I	0.485	I	0.485	2.75
Cement type	V	0.485	–	V	0.485	V	0.485	2.75
w/c	I	0.435	–			I	0.435	2.75
Presence of aggregate	I	0.485	0.2					

third-generation synchrotron facility at Argonne National Laboratory in Argonne, Illinois. For the reported measurements, the undulator gap was set to 19 mm and a taper of 5 mm was employed. The Bragg angle (2θ) was 2° , enabling diffraction peaks to be measured in the d -spacing range 12–3 Å (30–120 keV). The ability to measure relatively large d -spacing peaks using high-energy penetrating photons is important for the positive identification of ettringite and monosulfate phases in these samples.

One of the most significant features of EDXRD is that the incident and diffracted X-ray beam collimation defines a spatially fixed ‘gauge volume’ where the lines of sight of the incident and diffracted beam collimators intersect. Only material inside this volume contributes to the diffraction patterns, so diffraction data can be obtained as a function of position inside a sample by moving the sample between diffraction pattern acquisitions. In the present work, the cylindrical cement paste samples were mounted vertically and traversed in 50- μm steps along the radii of the cylinders. Both the incident and diffracted beams were collimated to 50 μm in the horizontal plane, leading to good spatial resolution (features less than 200 μm could be resolved). The diffraction patterns, recorded from different points along the sample radii, were processed to give composition depth profiles showing how the amount of each major crystalline phase in the sample changed as a function of depth below the sample surface. Further details regarding the experimental arrangement and data processing can be found in Ref. [16].

EDXRD measurements were made primarily on Type I and Type V cement paste samples with w/c of 0.485, although some measurements were made on Type V cement paste samples with w/c of 0.435. All data were recorded close to the middle of cylindrical specimens to avoid end effects. In many cases data were taken at two different distances from the end of the cylinder to check sample uniformity. The samples for study by EDXRD were selected on the basis of our μCT measurements.

3. Results and discussion

3.1. Influence of cement composition

The influence of cement composition on changes in engineering properties under sodium sulfate attack was investigated by monitoring expansion of Portland cement mortar bars and by measuring compressive strength of Portland cement paste cubes prepared from Type I and V cement. The interpretation of this data is aided by microCT and EDXRD. All samples considered in this section were produced with w/c of 0.485, as described in Section 2.

Average mortar bar expansion values until an exposure time of 52 weeks are shown in Fig. 1. After an apparent latent period extending approximately 13 weeks into the exposure, the Type I bars expanded more rapidly as compared to the Type V samples. At 52 weeks of exposure, the average expansions for Type I bars were 2.09%, while the Type V bar average expansion was 0.45%. In general, the standard deviations increased with time for the Type I bars, but such behavior with time was less apparent in the Type V bars. This increase in standard deviation with exposure may result from the inhomogeneities (e.g., cracking, spalling) induced in the samples during sulfate exposure leading to increased variations in the measurements among the different mortar bars of the same type.

In general, the expansion associated with sulfate attack is believed to largely result from the formation of ettringite due to the reaction of ingressing sulfate with existing hydration products (i.e., monosulfoaluminate hydrates, calcium aluminate hydrates) and with residual, unreacted phases (i.e., tricalcium aluminate or C_3A and tetracalcium aluminoferrite or C_4AF). The formation of gypsum, from the reaction of ingressing sulfates with calcium hydroxide, may produce some expansion, but the formation of ettringite is viewed as the more predominant cause (see Ref. [3], for example). The composition differences between the Type I and Type V cement and the resulting variations in types and

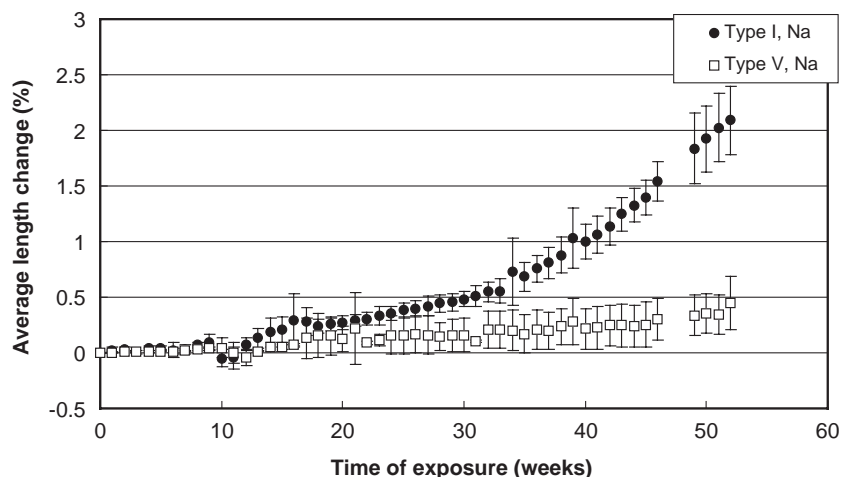


Fig. 1. Influence of cement composition on average expansion of mortar bars under sodium sulfate attack.

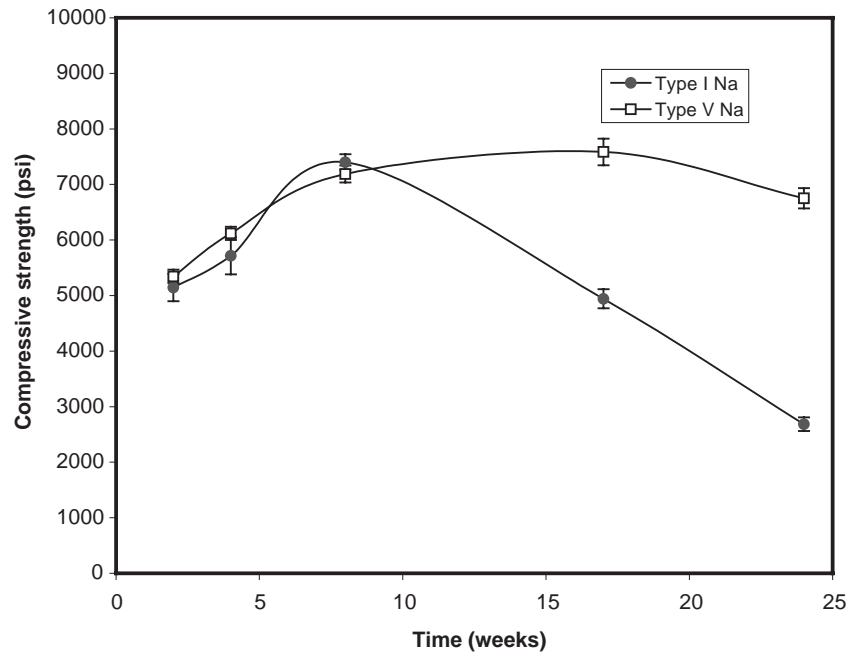


Fig. 2. Influence of cement composition on compressive strength with exposure to sulfate concentration of 10,000 ppm in sodium sulfate solution; trend lines shown as a guide to the eye.

relative amounts of hydration products are likely responsible for the differences in mortar bar expansion measured with continuing exposure.

First, the greater C_3A content in the Type I cement as compared to the Type V cement (9.9% vs. 3.3%) will influence the relative amounts of ettringite and monosulfate initially formed on hydration, and hence the propensity for later expansion by ettringite formation upon sulfate exposure. In addition, any unhydrated C_3A remaining may also result in ettringite formation and expansion, although EDXRD did not indicate the presence of any unhydrated C_3A in our samples.

Secondly, the potential effect of the greater relative amount of C_4AF in the Type V cement as compared to the Type I cement (11.1% vs. 8.2%) needs to be considered. Due to the greater quantity of C_4AF , ettringite formed in Type V cement samples during sulfate attack is likely to be

Fe-substituted. Iron-substituted ettringite is believed to be non-expansive or less expansive [17,18]. Thus, the lower C_3A content and the likelihood of ettringite being Fe-substituted are factors that may have contributed to the lower expansion observed in the Type V mortar bars.

Thirdly, the lower ratio of tricalcium silicate to dicalcium silicate (i.e., C_3S/C_2S) of the Type V cement is also likely contributing to its superior sulfate resistance as measured by expansion and changes in strength with exposure (discussed next). The ratio for Type V cement was 2.24 as compared to 10.81 for the Type I cement. There is evidence that sulfate-induced damage is linked, in some cases, to cements with higher C_3S content [4,19].

Average compressive strength measured for Types I and V cement pastes up to 24 weeks of exposure are shown in Fig. 2. For comparison, average 14-day compressive strengths for control samples (i.e., samples retained in

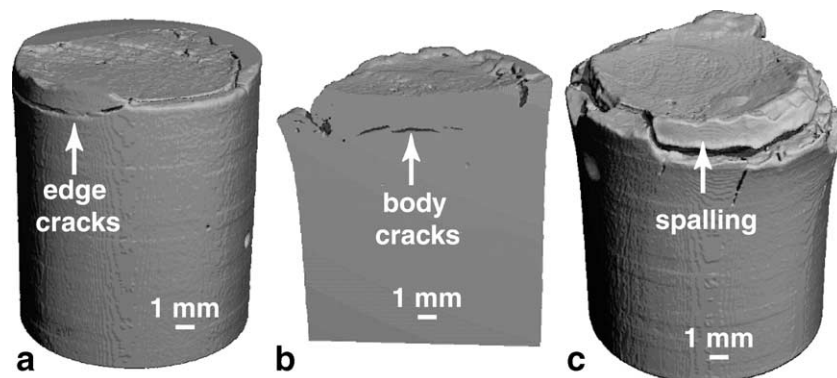


Fig. 3. Type I cement sample at $w/c=0.485$ and exposed to sulfate concentration of 10,000 ppm in sodium sulfate solution showing: a) edge cracks at 17 weeks, b) spalling and body cracking at 42 weeks, and c) continued spalling at 52 weeks of exposure.

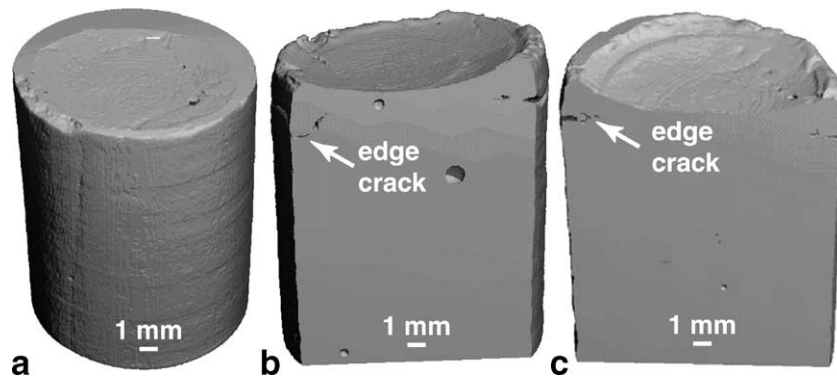


Fig. 4. Type V cement sample at $w/c=0.485$ and exposed to sulfate concentration of 10,000 ppm in sodium sulfate solution showing: a) no damage at 17 weeks, b) edge cracking at 42 weeks, and c) continued edge cracking at 52 weeks of exposure.

saturated limewater bath for 2 weeks beyond the initial 3-days curing) were 7000 psi and 5850 psi for the Type I and V cement pastes, respectively. Until 8 weeks of sulfate exposure, the average compressive strengths increased for both the Type I and Type V cement paste samples, as compared to the average compressive strengths after 2 weeks of exposure. The increase in average compressive strength until 8 weeks of exposure for both Types I and V cement samples may be expected due to the continued hydration of the samples in the sulfate solutions [11] and pore filling by the reaction products of sulfate attack [20]. However, by 17 weeks of exposure, the average compressive strength of the Type I cement samples had decreased to 4940 psi, while in the Type V cement samples continued to increase to 7500 psi. By 24 weeks, the strength of the Type I samples further decreased to 2680 psi, and the first decrease in strength for the Type V samples was noticed ($f_c=6750$ psi). These results show clearly the superior resistance of the Type V cement in terms of retention of compressive strength during sulfate exposure.

MicroCT was used to track the evolution of physical damage in corresponding Types I and V cement paste cylinders exposed to sodium sulfate solution. Figs. 3(a–c) and 4(a–c) show three-dimensional reconstructions of the top half of Type I and V specimens, respectively, after 17, 42 and 52 weeks exposure. These reconstructions of the Type I sample show that edge cracking (cracks near the sample edge) (Fig. 3a), was followed by body cracking (Fig. 3b) and spalling (Fig. 3c). Reconstructions of the Type V sample show no physical manifestations of damage at 17 weeks (Fig. 4a), but after 42 and 52 weeks exposure some cracking at the sample edge is apparent (Fig. 4b and c). Physical damage was first observed at 17 weeks in the Type I sample as compared to the Type V sample, where cracking at the edges was first observed after 26 weeks of sulfate exposure. Body cracking was first evident during microCT imaging at 36 weeks for the Type I sample, but was not apparent until 52 weeks in the Type V sample. Also, spalling at the sample edges was first observed at 42 weeks of exposure in the Type I cement paste sample, but has not been observed in the Type V cement paste sample after 78

weeks of exposure. Thus, in addition to the earlier appearance of these forms of damage in the Type I sample, the rate of damage progression was more rapid for the Type I cement paste sample.

Spatially resolved EDXRD data has been collected for both controls (i.e., samples stored in air-tight containers after the initial curing period) and sulfate-exposed samples (i.e., samples exposed to sulfate solution after the initial curing period). Fig. 5 shows, for Type I and Type V cements, the relative amounts of ettringite and monosulfate hydrate as a function of depth and exposure time in the samples before sulfate exposure and after 52 weeks in sodium sulfate solution.¹ Monosulfate hydrate was observed as the 12-water form ($\text{Ca}_4\text{Al}_2\text{O}_6(\text{SO}_4)\cdot 12\text{H}_2\text{O}$ or “12-water monosulfate”) and/or 14-water form ($\text{Ca}_4\text{Al}_2\text{O}_6(\text{SO}_4)\cdot 14\text{H}_2\text{O}$ or “14-water monosulfate”). In Fig. 5(a), all the curves for ettringite are on the same relative scale as one another, enabling a quantitative comparison between different exposure times and cement types, assuming that any variation in ettringite composition between the samples leads to minimal variation in the structure factor of the diffraction peak used to generate this data. Due to experimental limitations, the relative scales for the ettringite and 12-water and 14-water monosulfate hydrate are not the same, and quantitative comparisons describing the relative amounts of the phases in relation to one another cannot be made. That is, quantitative comparisons can only be made when examining the same phase in different samples, *not* when comparing different phases within the same or different samples.

As expected due to the higher C_3A content of the Type I cement, the Type I control contains more ettringite and monosulfate than the Type V control. Very little monosulfate is detected in the Type V cement control, as would be expected [21–23]. In the Type I control both the 12 and 14-water forms of monosulfate are detected; it is well

¹ Crystalline Na-bearing phases are not observed in either the Type I or Type V samples. This observation is consistent with the previous observation that very little Na can be detected in Na_2SO_4 attacked pastes beyond the near-surface region (Gollop and Taylor, 1992).

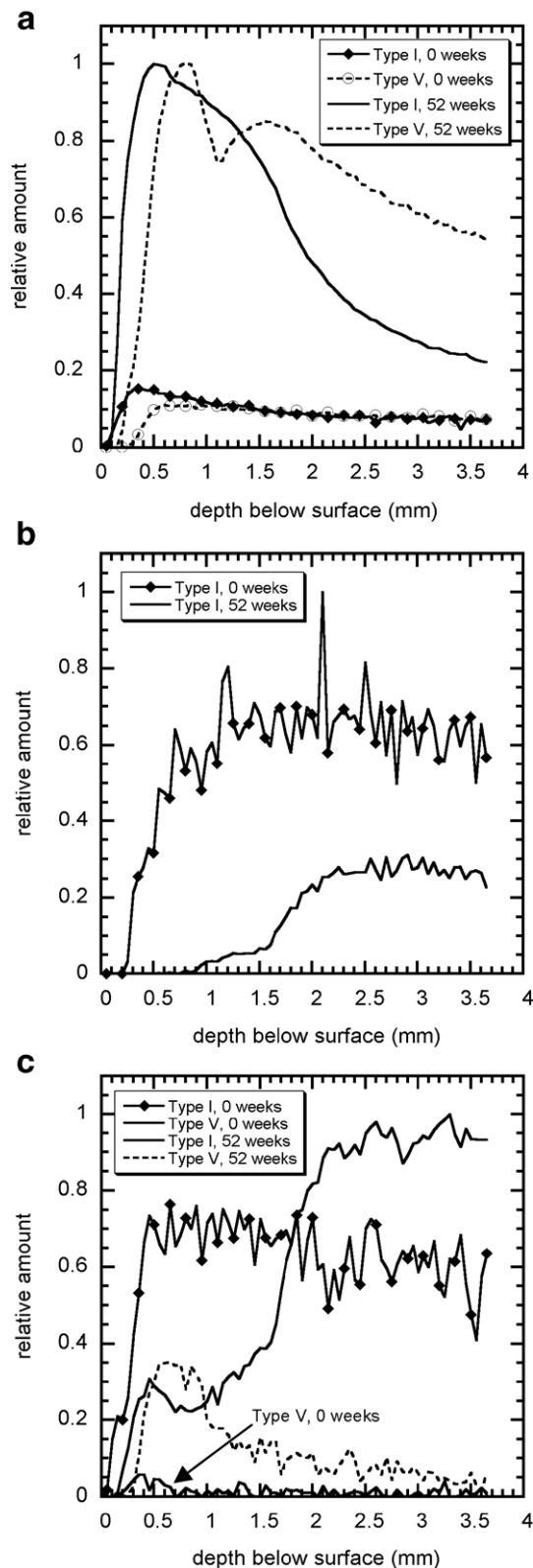


Fig. 5. Relative amounts of a) ettringite, b) monosulfate 12-hydrate and c) monosulfate 14-hydrate observed in specimens exposed to 10,000 ppm sodium sulfate solution for 52 weeks are compared to those found in the corresponding controls. Within each panel, the plots are on the same relative scale enabling a quantitative comparison between the amounts of a given phase in different specimens.

known that these monosulfate phases can react during sulfate attack to form ettringite (see, for example, Ref. [3]). After 52 weeks of exposure, however, the maximum amount of ettringite observed in both the Type I and Type V samples is remarkably similar, which was not expected based on data in the literature [24]. As there was much less monosulfate in the Type V control than the Type I control, with no observation of unhydrated C_3A , and no obvious corresponding depletion of C_4AF , the data suggests that aluminum for ettringite formation in the Type V sample might be coming from a source other than monosulfate and residual unhydrated phases. Gollop and Taylor [21–23] report the close admixture of Al^{3+} in calcium silicate hydrate (C–S–H), and it seems possible that this is a potential source of Al^{3+} for continued ettringite formation in the absence of observable depletion of crystalline Al-bearing phases.

The ettringite curves for the Type I and V cement pastes after 52 weeks sulfate exposure (Fig. 5(a)) show marked differences when comparing the relative amounts of ettringite detected near the sample surface (~ 0 –1.5 mm) and at greater depths (~ 2.5 –3.5 mm) in each sample. The ettringite concentration varies much more with depth in the Type I sample than in the Type V sample. This observation, which is also true for the ettringite depth profiles of Type I and V samples subject to other sulfate exposure durations, is perhaps consistent with a somewhat different mechanism for the formation of ettringite in the two samples. If the ettringite formed in these samples leads to expansion, the much stronger variation of ettringite concentration as a function of depth in the Type I sample when compared to the Type V sample, likely leads to different stress states in the two types of samples.

In Fig. 6(a), EDXRD composition-depth profiles for a Type I cement paste control sample are presented. Crystalline phases typically resulting from cement hydration, including ettringite, monosulfate, and calcium hydroxide, are identified throughout the 4-mm depth interrogated. Ettringite is present in greater quantity near the surface of the specimen, in a region where there appears to be a corresponding decrease in the amount of 12-water monosulfate, relative to that observed at greater depths. The data for calcium hydroxide perhaps indicates that some very near-surface depletion has occurred. The considerable point-to-point fluctuations in the $Ca(OH)_2$ data are due to the relatively large size of those crystals compared to the volume sampled in the EDXRD experiment. In addition, there was evidence for unhydrated C_4AF throughout the depth examined; this data has not been included to simplify the data presentation in this figure.

The corresponding composition profiles for a Type I specimen after 52 weeks of sodium sulfate exposure are shown in Fig. 6(b). Both the monosulfate phases are further depleted in the near-surface region, relative to observations of these phases in the control sample (Fig. 6(a)). In the region where the monosulfate is depleted (first ~ 1.5 mm), the amount of ettringite is much greater than found in the

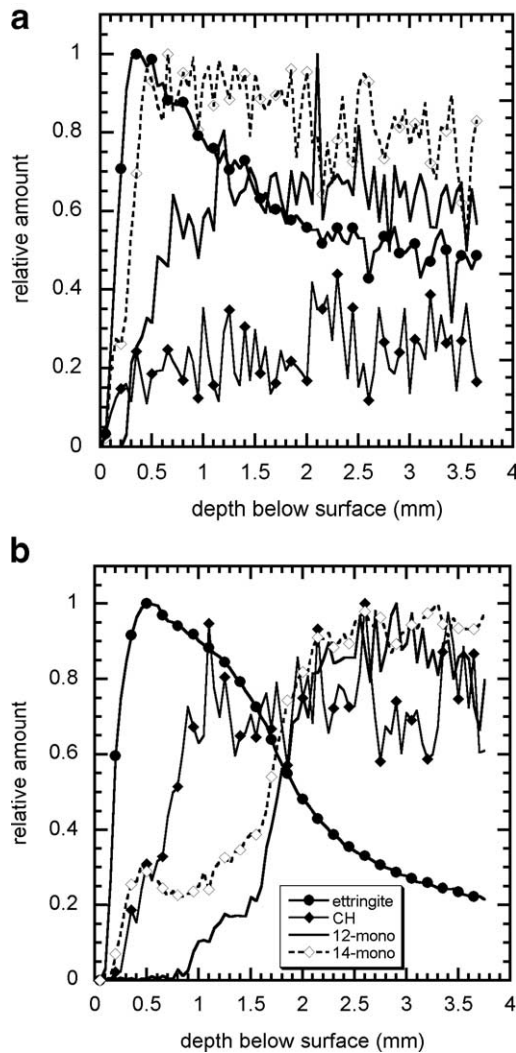


Fig. 6. Composition depth profiles from EDXRD for Type I cement paste samples with w/c of 0.485 a) in control sample and b) in exposed sample after 52 weeks exposure to 10,000 ppm sulfate solution. The legend in 6(b) serves for both figures. As the scaling of the lines in the two panels has been chosen to best illustrate the spatial relationships between the various phases, it is not possible to quantitatively compare the amounts of the different phases within a panel or between panels.

control, clearly suggesting the well-known progressive reaction of monosulfate to form ettringite as sulfate diffuses into the sample. After 52 weeks of sulfate exposure the near surface region is clearly depleted in calcium hydroxide to a depth of over 0.5 mm. It is notable that *no gypsum* is detected in the Type I sample at 52 weeks of sulfate exposure.

In Fig. 7(a), composition depth profiles for a Type V control samples are presented. As in the Type I control sample (Fig. 6(a)), crystalline products of hydration, including ettringite, monosulfate (here, detected as 14-water monosulfate only), and calcium hydroxide, as well as some unhydrated C_4AF , present throughout the sample depth, are detected. As with the Type I control sample, the amount of ettringite near the sample surface is greater relative to the interior of the sample.

Fig. 7(b) presents the corresponding profiles for a Type V paste sample after 52 weeks of exposure to sodium sulfate solution. No 12-water monosulfate hydrate is detected in this sample, and the small amount (see Fig. 5(b) for comparison with other samples) of 14-water monosulfate present appears to be concentrated near the surface in a region that is substantially free of calcium hydroxide. One remarkable feature of this data is the near-surface depletion of calcium hydroxide, which occurs to a much greater depth than was observed in the 52-week Type I specimen. This difference is possibly related to the lower C_3S/C_2S in the Type V cement, which would then result in less calcium hydroxide initially produced by cement hydration as compared to the Type I and is likely also related to the consumption of $Ca(OH)_2$ in chemical reactions with the ingressing sulfates to form, for

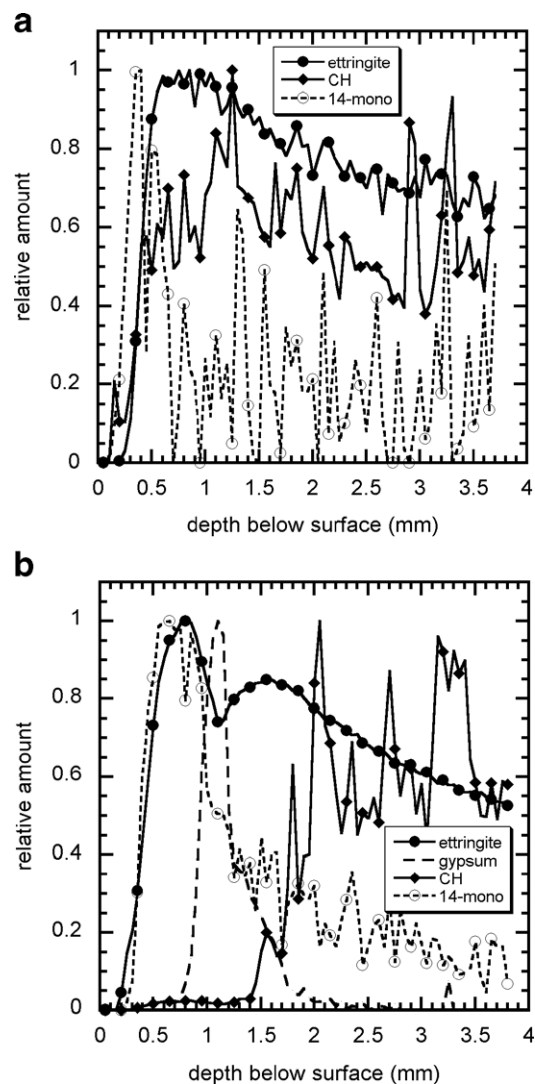


Fig. 7. Composition depth profiles from EDXRD for Type V cement paste samples with w/c of 0.485 a) in control sample and b) in exposed sample after 52 weeks exposure to 10,000 ppm sulfate solution. As the scaling of the lines in the two panels has been chosen to best illustrate the spatial relationships between the various phases, it is not possible to quantitatively compare the amounts of the different phases within a panel or between panels.

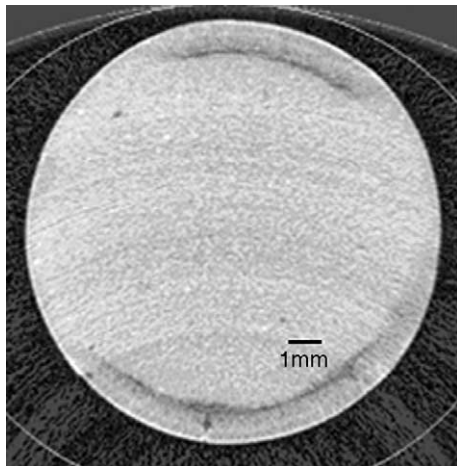


Fig. 8. Ring cracks are observed by microCT at ~ 0.9 mm depth in Type V cement samples with w/c of 0.485 after 64 weeks exposure to sodium sulfate solution.

example, gypsum and ettringite. Thus, it is also notable that in the near-surface region a band of gypsum is observed at ~ 1 mm below the surface. The curves for gypsum and ettringite in this region are clearly anticorrelated in this sample; similar behavior was also observed for other Type V specimens with different sulfate exposure times and with different sulfate solution concentrations [25]. Previously, it has been suggested that gypsum, rather than ettringite, forms when SO_4^{2-} is available, but the available Al^{3+} has been consumed [3]. However, the anticorrelation between gypsum and ettringite seen in the present data does not agree with this. It is possible that some of the ettringite originally present in the 52 week sample at 0.7–1.5 mm depth decomposed to form gypsum and perhaps other products which were either non-crystalline or not detectable for other reasons. The decomposition of expansive ettringite into gypsum, if accompanied by strain recovery, could change the local stress state and lead to cracking.

There is literature [7,26,27] indicating that the decomposition of ettringite to gypsum may be related to a decrease in pH and in all our specimens, gypsum was only observed in regions that were substantially free from calcium hydroxide. Although $\text{Ca}(\text{OH})_2$ has been depleted in the 1.4 mm nearest the surface for our 52-week Type V sample the detection of ettringite very near to the sample surface (Fig. 7(b)) gives evidence that the pH remains high enough for ettringite stability in this region. This suggests that either the pH profile between the sample surface and the region still containing $\text{Ca}(\text{OH})_2$ is complex or that the anticorrelation between the ettringite and gypsum curves is not driven by pH. Another possible explanation is that the ettringite partly converts to gypsum due to high local sulfate concentrations. This behavior has been predicted in a study examining the stability of ettringite in alkaline environments as a function of pH and sulfate ion concentration [28]. Also, sodium ions suppress the solubility of $\text{Ca}(\text{OH})_2$ and increase the solubility of gypsum. This influence on pH of pore solution needs also to be examined.

The anticorrelation between the gypsum and ettringite profiles could also be interpreted as an indication of gypsum crystals depositing into preexisting cracks in the cement paste. The microCT data has sometimes shown cracks parallel to the sample surface (i.e., “ring” and/or “longitudinal” cracking) at the depth where EDXRD shows that the first gypsum band begins. That is, the presence of gypsum seems to be sometimes associated with ring or longitudinal cracking. For example, in Fig. 8 a crack is observed at 64 weeks at a depth of ~ 0.9 cm, which closely matches the location of a band of gypsum at 52 weeks (Fig. 9). However, comparison of microCT slices and 3D renderings with corresponding EDXRD data for the same volume of cement paste does not fully corroborate this theory of gypsum product formation within cracks. Specifically, gypsum has been observed in samples *prior* to the observation of a crack; also, gypsum is seen in samples displaying no obvious cracking by microCT; and, finally, the location of the gypsum band locations migrate inward with time (see Fig. 9, discussed next). Each of these observations suggests that cracks may not be required for gypsum formation. However, the limitations of the techniques used must also be considered: it is possible that radial cracks too small to be discernible by microtomography may exist [21–23], and with EDXRD, the thickness of a gypsum band can be reliably estimated only if it lies nearly parallel to the sample surface. While it can be difficult to distinguish if the gypsum is forming within a crack (when one is observed) or in the adjacent paste, the cracks that are observed seem to be of insufficient thickness to accommodate deposits of gypsum of the thicknesses suggested by the EDXRD. Thus, cracking followed by gypsum crystallization in the cracks does not seem fully consistent with the data. Rather, it appears as though much of the gypsum exists or forms in the paste near the crack, when cracks are present.

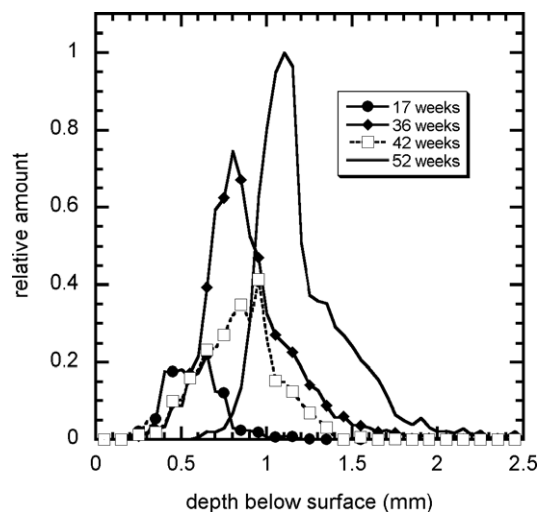


Fig. 9. Gypsum concentration profiles as a function of sulfate exposure time as seen by EDXRD for a series of Type V cement paste samples with w/c of 0.485. All data are on the same relative scale permitting quantitative comparison.

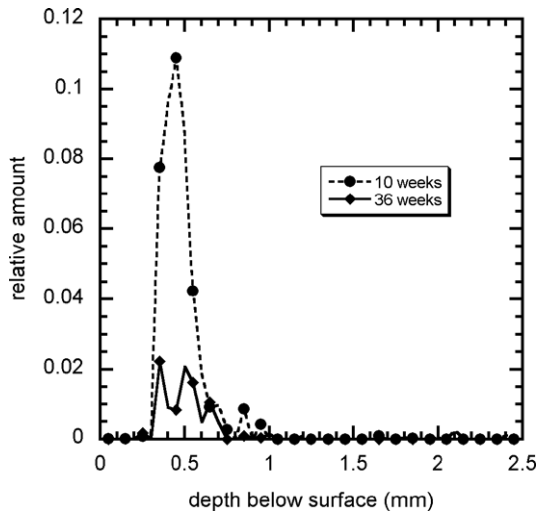


Fig. 10. Gypsum concentration profiles as a function of sulfate exposure time as seen by EDXRD for a series of Type I cement samples with w/c of 0.485. All data are on the same relative scale permitting quantitative comparison within this figure and with the data shown in Fig. 8. No gypsum was detected in Type I samples exposed for longer than 36 weeks.

In general, the pattern of gypsum formation has varied with cement type in the samples examined. As briefly mentioned previously, EDXRD data from Type V samples show that the gypsum-bearing zone migrates inwards over time (Fig. 9) and that the total amount of gypsum in the sample increases with time. In marked contrast, in Type I samples exposed to the same sulfate-attack conditions, the gypsum layer makes only a transient appearance. A relatively small amount of gypsum forms at a depth of ~ 0.5 mm below the surface after 10 weeks, but at 36 weeks very little remains, and no inward migration has taken place (Fig. 10). Surprisingly, after 42 weeks exposure or more, no gypsum was observed in the Type I samples. The behavior of both sample types suggests that once gypsum has been

deposited it can later re-dissolve or react to form other products. However, in the case of the Type V samples as the gypsum in the near surface region is depleted more gypsum is formed at greater depths, but in the Type I samples no new gypsum crystallites are deposited at greater depths. Further research is clearly necessary to better understand the role of gypsum in sulfate deterioration.

3.2. Influence of w/c

Concrete and cement paste with lower w/c has been shown to possess greater resistance to sulfate attack (see Refs. [1–4], for example). Previously, microCT characterization of pastes at w/c of 0.45, 0.50, and 0.60 showed that the onset of sulfate damage (in 10,000 ppm sulfate in Na_2SO_4 solution) was more rapid at higher w/c [14]. As a result of this understanding, various agencies (e.g., ACI, CEMBUREAU, etc.) make recommendations regarding maximum w/c for anticipated exposure conditions, as well as other requirements for cement composition, use of supplementary cementitious materials, and strength. As the severity of the sulfate exposure condition increases, the recommended maximum w/c in concrete decreases. Here, the influence of w/c was investigated by examining expansion of Type I Portland cement mortar bars and comparing these results with the damage to cylindrical Type I Portland cement paste samples, as measured by microCT. Two w/c were examined — 0.485 and 0.435.

In the present study, expansion of Portland cement mortar bars under sodium sulfate attack was greater for higher w/c (Fig. 11), which is in line with the expected behavior for concrete. Until about 12 weeks of exposure, average expansions were similar in both cases. Beyond this period, the average length change increased more rapidly for the samples with the higher w/c . Average expansion at 52 weeks was much greater for the higher w/c samples, as expected.

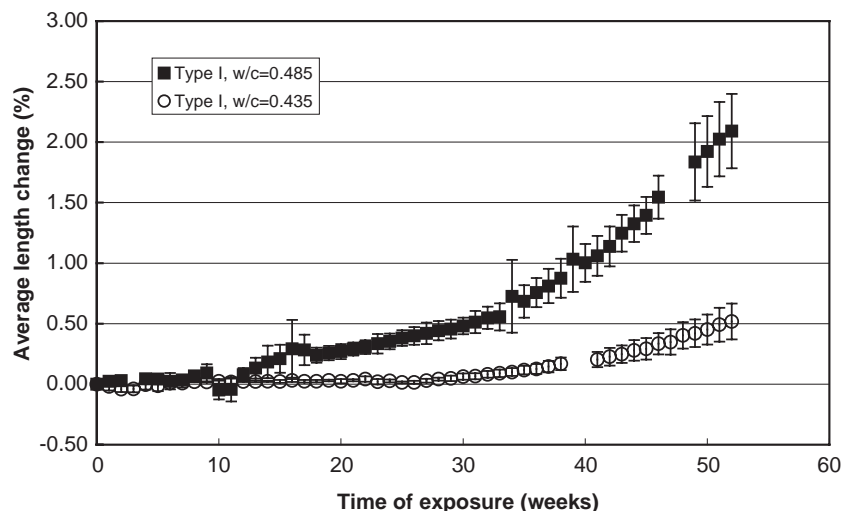


Fig. 11. Influence of w/c on average expansion of mortar bars under sodium sulfate attack.

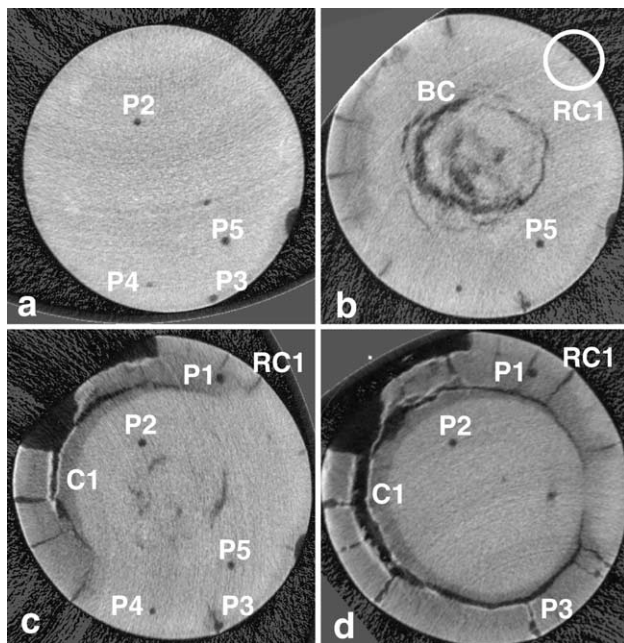


Fig. 12. Matching slices of a Type I cement paste sample at w/c of 0.485 and exposed to 10,000 ppm of sulfate ions in sodium sulfate solution after a) 21 weeks (slice number 70), b) 36 weeks (slice number 108), c) 42 weeks (slice number 71), and d) 52 weeks (slice number 79), and showing crack C1, radial crack RC1, and pores P1–P5. The horizontal field of view is a) 15.3 mm, b) 15.1 mm, c) 16.1 mm, and d) 15.2 mm.

When comparing expansion data in Figs. 1 and 11, it is notable that a decrease in w/c from 0.485 to 0.435 (with Type I cement) and the substitution of Type V cement (with w/c of 0.485) for Type I both produce similar decreases in mortar bar expansion, as compared to Type I bars with w/c of 0.485. However, the initial latent period when very little expansion was observed, was much shorter for the Type V cement samples (about 13 weeks) than for the Type I lower w/c samples (27 weeks). This similarity in performance shows that there exists some flexibility in the design of economical Portland cement mortar mixtures resistant to sulfate attack. The disparity in the latent period also shows the need for longer monitoring of expansion samples to gauge performance.

MicroCT was used to image the physical manifestations of damage in cylindrical cement paste samples at w/c of 0.485 and 0.435. While the expansion data generally agrees with expected behavior with changing w/c , the physical damage observed in cylindrical cement paste samples by microCT was more severe at the lower w/c . This result was unexpected.

Volumetric reconstructions of a Type I cement paste sample at w/c of 0.485 and exposed to sodium sulfate solution for 17, 42, and 52 weeks have been shown in Fig. 3 and were discussed in Section 3.1. Observations of the same 2-D slice over time allow the evolution of damage in a sample to be tracked. Slight variations of tilt in the sample within the microCT 40 sample holder produced slight variations in the closest matching slices; thus, pre-existing

voids in the sample were used as fiducials to establish matching slices in the samples over time. Fig. 12(a–d) shows the matching slices, where fiducial voids or pores have been labeled P1–P5, at 21, 36, 42, and 52 weeks of exposure for the same sample. At this position near the end of the sample, no damage was observed at 21 weeks (Fig. 12(a)). At 36 weeks (Fig. 12(b)), a surface radial crack (RC1) has just begun to form; some body cracks in the middle of the slice are also present. In Fig. 12(c) the body cracks are barely visible (in fact in this data set, 42 weeks exposure, the main portions of the cracks lie slightly above the plane of the slice); and in Fig. 12(d), 52 weeks exposure, solid body displacement of the central core relative to the outer shell (i.e., along the cylinder's axis) has brought the body cracks farther from the slice shown. At 42 weeks of exposure (Fig. 12(c)), the width of RC1 has widened to 0.16 mm; spalling was observed and a ring crack (C1) had a width of 0.26 mm. At 52 weeks of exposure (Fig. 12(d)), the width of RC1 has grown to 0.22 mm; some spalling continues, and the width of C1 measures 0.68 mm.

Near the ring crack C1 at 42 weeks (Fig. 12(c)) and 52 weeks (Fig. 12(d)), a very dense region (i.e., lighter pixels) was observed at the crack surfaces. The very dense region at the crack surfaces had a linear attenuation coefficient of about 2.4 cm^{-1} at 42 and 52 weeks of exposure, which is greater than the 1.6 to 2.2 cm^{-1} measured elsewhere in the sample. The linear attenuation coefficients were measured as an average of five values near the position shown. The exact underlying cause for the formation of the very dense region at the crack surfaces is not clear, but it is likely that reaction products are forming in this region due to reaction with the ingressing sulfate solution.

Immediately adjacent to this dense region toward the sample core, a less dense region (darker in color), as compared to the sample core, was observed. The linear attenuation coefficient of the less dense region adjoining C1 was 1.3 cm^{-1} and the thickness of this region was 0.7 mm at 42 weeks of exposure; for the same less dense region at 52 weeks of exposure, linear attenuation coefficient was 1.5 cm^{-1} and thickness was 0.8 mm. The less dense region adjoining the crack is believed to be due to leaching of calcium hydroxide, decalcification of C–S–H, or some other dissolution process resulting from exposure to the external solution at the cracked surfaces.

Fig. 13 shows volumetric renderings at 9, 16, 22 and 32 weeks of exposure for the same Type I Portland cement sample at the lower w/c of 0.435. At 9 weeks, the first physical manifestation of damaged edges – cracking at the edges – was observed. It is notable that the first physical manifestations of damage are apparent earlier, at 9 weeks vs. 17 weeks (for the w/c of 0.485), in the lower w/c sample. By 16 weeks of exposure, damage had progressed significantly: existing cracks have widened and new cracks have formed (body cracks were first apparent at 13 weeks). MicroCT at 22 weeks of exposure shows continued crack growth and the first observation of longitudinal cracks along

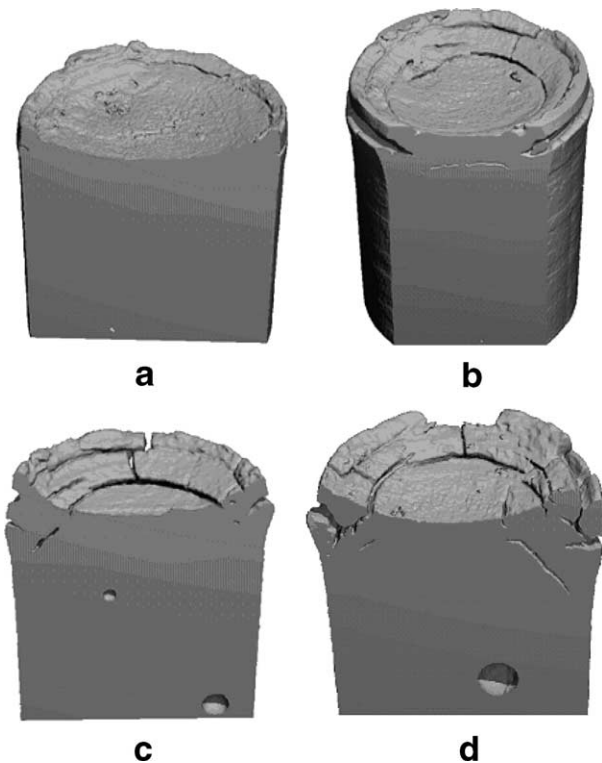


Fig. 13. 3D renderings of Type I cement paste sample at w/c of 0.435 and exposed to 10,000 ppm of sulfate ions in sodium sulfate solution for a) 9 weeks showing onset of cracking at the edges, b) 16 weeks showing widening of existing cracks and formation of new cracks, c) 22 weeks showing continued cracking, and d) 32 weeks showing increased cracking and spalling.

the sample surface (not visible in the image shown). At 32 weeks, cracking and spalling were more extensive than at earlier times. The low w/c cement paste samples com-



Fig. 15. Type I cement paste samples with w/c of 0.485 showed multiple cracks and some spalling at 108 weeks of exposure.

pletely disintegrated after 56 weeks of exposure. Interestingly, each of the samples of this type subjected to this exposure broke at approximately mid-height, with relatively flat fracture surfaces (Fig. 14). At the sample ends, expansion and cracking can be noted. This flat fracture surface with the observation of cracking and expansion in the sample seems to suggest the development of tensile stress along the long axis of the sample, leading to brittle, localized failure. (For comparison, an entirely different pattern of cracking is noticed for the 0.485 w/c samples, Fig. 15, which remain largely intact, but heavily cracked, at 108 weeks. The presence of multiple cracks, running longitudinally and radially, in the higher w/c samples suggests a more multiaxial state of stress.)

The earlier appearance of damage and the more rapid failure (i.e., disintegration) of the lower w/c cement paste

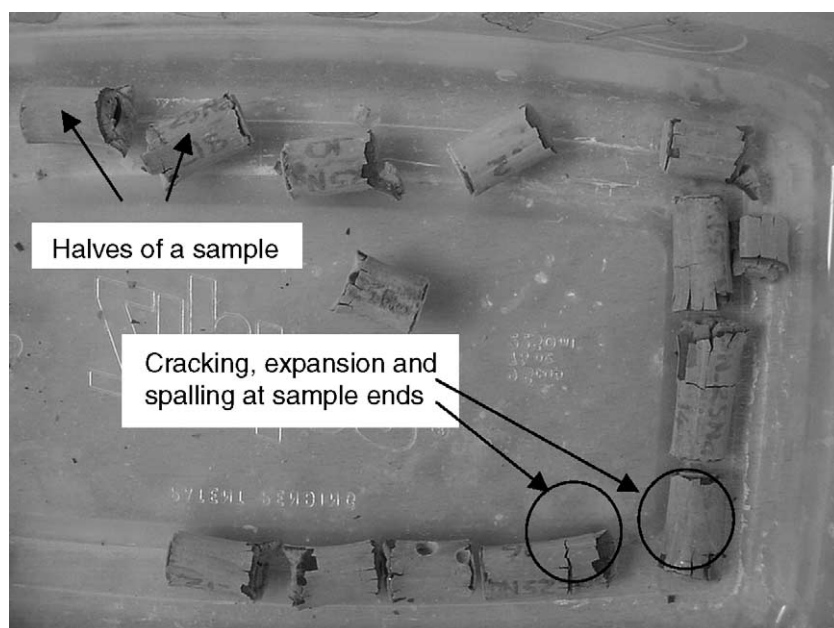


Fig. 14. Type I cement paste samples with w/c of 0.435 exhibited cracking and broke into halves at 56 weeks of exposure.

warrants further discussion. The potential effects of reduced workability, degree of hydration, changes in extensibility, and pore structure were considered. As described in detail by Naik [25], analysis of the microtomography data showed only a small difference in void volume fraction (0.4% air at w/c of 0.485 vs. 2% at 0.435) between the samples prior to exposure, indicating that variations in workability likely had no major role in the unexpected behavior of the cement paste samples at the lower w/c . The potential influence of a greater amount of unhydrated or residual C_3A at lower w/c was also considered. However, as no residual C_3A was detected by EDXRD in the samples at any age, the role of unhydrated C_3A is likely minor, if contributing at all.

Rather, it is proposed that changes in extensibility and pore structure are more likely factors resulting in earlier cracking in failure in the lower w/c cement paste samples. As w/c decreases, the compressive strength and elastic modulus of concrete or cement paste increases [29]. In such materials, the tensile strength may also be higher than in normal strength concrete or paste, but the relative increase in tensile strength does not scale with the relative gains in compressive strength and stiffness (i.e., gains in tensile strength are quite small, relative to increases in compressive strength and E as the w/c decreases.) This reduces the extensibility (i.e. ability to deform without cracking) of material. That is, for a given tensile elastic strain, with increasing stiffness, the tensile stress induced will increase. Thus, given that the extensibility would be decreased as w/c decreases, it might be expected that cracking would occur earlier in those samples, as was observed here. The observation of flat fracture surfaces at the lower w/c (Fig. 14) – a pattern which is indicative of tensile failure in brittle samples – substantiates the likelihood of the role of decreased extensibility in these samples.

Changes in the pore structure with decreasing w/c should also be considered. With a reduction in w/c , the microstructure of hardened cement paste is refined and pore sizes generally decrease. Measurements of linear attenuation during X-ray microtomography have suggested that the voids in the pastes become filled with material during sulfate attack [15,25]. Scherer [30] has considered damage

resulting in brittle materials by crystallization in pores. Among other factors, Scherer reports that greater stresses are developed when crystallization occurs in pores of smaller size. Hence, reductions in w/c , while improving impermeability, may produce a microstructure *in cement paste* (i.e., in the absence of aggregate), that is more prone to damage once crystalline sulfate attack reaction products begin to form in the pores.

It is also to be emphasized that samples examined herein were small, unrestrained, and unreinforced cement pastes. The small size and lack of restraint or reinforcement was selected to accelerate the onset and progress of damage, as compared to concrete structures in practice.

3.3. Influence of presence of aggregate

In addition to examining neat cement pastes, sulfate-induced damage to Type I cement samples at w/c of 0.485 containing quartz aggregate particles were characterized by microCT. Fig. 16 shows progressive damage to a sample containing aggregate after 7, 17, and 21 weeks of exposure, for comparison with a compositionally similar sample (without aggregate) in Fig. 3. The aggregate are apparent as irregularly shaped inclusions, which appear in these 3D renderings like void space. The first appearance of physical damage in samples containing aggregate was in the form of edge cracks noted after 12 weeks of exposure. By 16 weeks exposure, cracks running along the length of the sample (longitudinal cracks) and body cracks were evident. By 17 weeks, extensive cracking and spalling at the edges and cracking within the sample body were evident, and further cracking and spalling was observed after 21 weeks exposure. The sample had completely disintegrated by 35 weeks.

For a detailed appreciation of damage evolution in these samples, microCT slices were examined (Fig. 17). While no damage was observed at 7 weeks of exposure, (Fig. 17(a)), at 17 weeks exposure (Fig. 17(b)) an interface crack partially surrounded aggregate particle AG1; body cracks BC1 and BC2 were present, with BC1 passing through the interface of cement paste matrix and aggregate

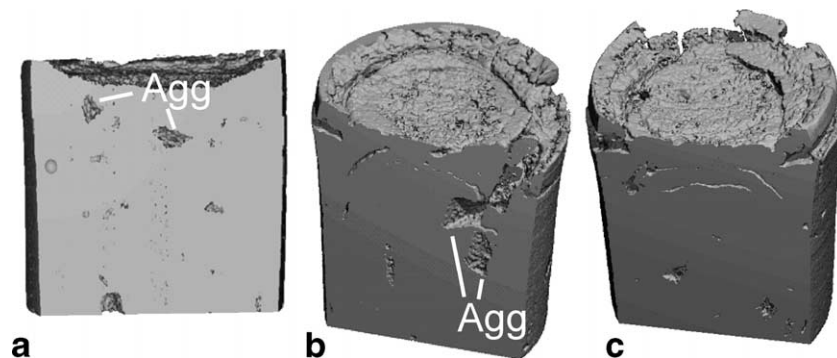


Fig. 16. Type I cement paste-aggregate sample at w/c of 0.485 and exposed to 10,000 ppm of sulfate ions in sodium sulfate solution for a) 7 weeks showing no damage, b) 17 weeks showing cracking and spalling at the edge and cracking within the sample body, and c) 21 weeks showing continued cracking and spalling.

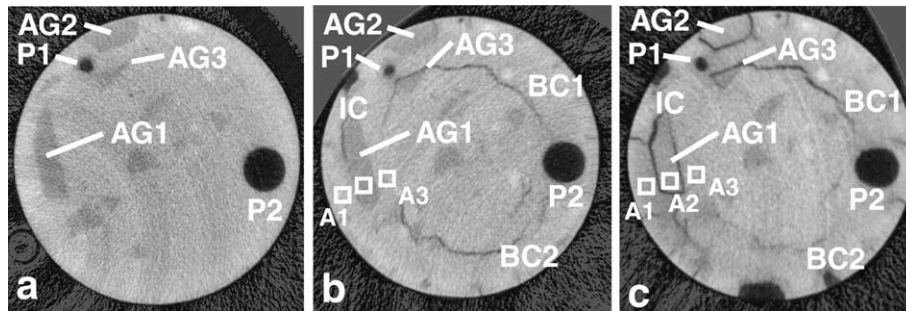


Fig. 17. Matching slice for Type I cement paste-aggregate sample at w/c of 0.485 and exposed to 10,000 ppm of sulfate ions in sodium sulfate solution for a) 7 weeks (slice number 88), b) 17 weeks (slice number 74), and c) 21 weeks (slice number 77), showing the presence of aggregate particles AG1–AG3, interface crack IC, body cracks BC1 and BC2, and pores P1 and P2. The horizontal field of view is a) 14.9 mm, b) 15.3 mm, and c) 16.8 mm.

particle AG3; radial cracks were also present. While no interface crack was observed around aggregate particle AG2 in this slice, a crack was present and linked to the surface at about slice number 60, i.e. closer to the end of the sample. A small amount of spalling was also observed. At 21 weeks exposure (Fig. 17(c)), the most notable change (compared to the matching slice at 17 weeks) was that aggregate particles AG1 and AG2 were completely outlined by interface cracks. The width of the interface crack at the position marked IC was 0.15 mm at 17 weeks and 0.23 mm at 21 weeks. Spalling was more severe and the radial cracks were more pronounced at 21 weeks than at 17 weeks. In addition, at 21 weeks of exposure, the linear attenuation coefficients of the cement paste matrix for area A1 near the sample surface ($=1.8 \text{ cm}^{-1}$) and region A3 near the sample core ($=1.8 \text{ cm}^{-1}$) were less than the linear attenuation coefficients in the same regions at 7 ($A1=2.7 \text{ cm}^{-1}$; $A3=2.1 \text{ cm}^{-1}$) and 17 weeks of exposure ($A1=2.4 \text{ cm}^{-1}$; $A3=2.3 \text{ cm}^{-1}$). Regions A1 and A3 in the cement paste matrix were in close proximity to the aggregate, AG1, which by this exposure time was completely surrounded by an interface crack linked to the sample surface. Dissolution of the matrix material in the regions close to the interface crack likely led to decreases in density in regions A1 and A3, with linear attenuation coefficient of the aggregate particle AG1 confirmed to remain constant with time.

As compared to the corresponding cement paste sample (i.e., at $w/c=0.485$ and exposed to 10,000 ppm of sulfate ions in a sodium sulfate solution), the progress of damage was more rapid in the cement paste-aggregate sample. Damage was first apparent by microCT in the sample containing aggregate at 12 weeks versus 17 weeks for the neat cement paste sample. At 17 weeks, damage in the cement paste-aggregate sample was much more extensive than in the absence of aggregate, as can be clearly seen comparing Figs. 16 and 3. In the presence of aggregate, body cracks and radial cracks were much more often linked to interface cracks, indicating that the cement paste–aggregate interface facilitated more rapid progression of damage than in the aggregate-free samples. Notably, the cement paste sample remained intact beyond 78 weeks of

exposure, while the cement paste-aggregate sample had completely disintegrated by 35 weeks.

Thus, as anticipated, the presence of aggregate appears to have accelerated both the initiation and progression of damage by sulfate attack. This is likely related to the increase in permeability associated with the cement paste/aggregate interface. Others have also suggested that the reaction of large calcium hydroxide crystals formed at the interface, during hydration, with ingressing sulfates to form gypsum (and, perhaps ettringite in the presence of aluminum) may also play a key role in the more rapid degradation of cement-based materials containing aggregate [31]. Further EDXRD measurements, with particular attention to the aggregate/paste interface, are necessary to assess the relative importance of these potential reactions as compared to the inherent increase in permeability.

4. Conclusions

Results from an integrated sulfate research program which includes X-ray microtomography (microCT), energy dispersive X-ray diffraction (EDXRD), and measurements of strength and length change have been presented to examine the influence of cement type, water-to-cement ratio, and the presence of aggregate on sulfate resistance. All samples were exposed to 10,000 ppm sulfate in Na_2SO_4 solution. This research has produced results which support some commonly held understanding of the mechanisms of sulfate-induced damage in cement-based materials, while other observations do not fit with current understanding; key observations in both areas are highlighted below. One outcome of this research, then, is clearly the need for further fundamental research to link the chemical, physical, and mechanical changes occurring in cement-based materials during reaction with sulfate solutions.

4.1. Effect of cement type

Considering the expansion, strength, microCT, and EDXRD data, it is clear that cement composition has a strong influence on resistance to sulfate distress, with the

Type V cement demonstrating greater resistance, as anticipated. That is, the Type V cement showed less expansion with exposure, no loss in compressive strength, later manifestations and slower progress of physical damage. These physical and mechanical differences are accompanied by chemical differences as seen by EDXRD including the observation that the shape of the ettringite depth profiles are distinct, with Type I showing more variation with depth. Another distinction with cement type is that at long sulfate exposure times gypsum is observed only in the Type V samples, where a band of gypsum is observed to “migrate” inward with continued exposure. The lower C_3A content, lower C_3S/C_2S , and higher C_4AF content are believed to be key factors influencing the improved resistance of Type V cement, as generally accepted.

Another interesting observation involves the relationships between the formation of gypsum and ettringite and the location of cracks, as detected by microCT, in a sample at 52 weeks of exposure. By EDXRD, an anticorrelation was observed between gypsum and ettringite. The data suggests that ettringite, with continuing sulfate exposure, has decomposed to form gypsum. With a crack detected very near the location in the paste where gypsum is formed, it is possible that a localized increase in sulfate ion concentration, due to localized increased permeability, may be a driving force for the formation of gypsum. However, the links between ettringite loss, gypsum formation, and cracking are not clear and should be examined further.

4.2. Effect of w/c

Under sodium sulfate attack, the onset and progression of physical deterioration (i.e., cracking, spalling, and disintegration) in cement paste specimens as detected by microCT occurred more rapidly at the lower w/c . These observations run counter to anticipated behavior and are not supported by measurements of expansion in mortar bar samples at the same two w/c values. For cement pastes, it was proposed that changes in extensibility and pore structure with decreasing w/c are likely factors contributing to the deterioration trends observed by microtomography.

4.3. Effect of aggregate

As anticipated, in the presence of aggregates a more rapid onset and progression of physical distress was observed. Damage was first apparent by microCT in samples with aggregate at 12 weeks sodium sulfate exposure, versus 17 weeks for the neat cement paste sample. Samples containing aggregate failed by 35 weeks exposure, while the corresponding cement paste samples had not completely disintegrated after 78 weeks exposure. In the presence of aggregate, body cracks and radial cracks were often linked to cracks at the paste/aggregate interface.

Acknowledgements

This research was supported by National Science Foundation (NSF) CMS-0084824. The microtomography equipment was acquired under NSF OIA-9977551. The EDXRD work was performed at the Advanced Photon Source which is supported by the Department of Energy under contract W-31-109-ENG-38. Any opinions, findings, and conclusions or recommendations expressed in this material are those of the authors and do not necessarily reflect the views of the sponsors.

References

- [1] P.K. Mehta, Sulfate attack on concrete — a critical review, in: J. Skalny (Ed.), *Materials Science of Concrete: III*. American Ceramic Society, 1992, pp. 105–130.
- [2] K.E. Kurtis, P.J.M. Monteiro, S. Madanat, Empirical models to predict concrete expansion caused by sulfate attack, *ACI Mater. J.* 97 (2) (2000) 156–161; Errata 97 (6) (2000) 713.
- [3] J. Skalny, J. Marchand, I. Odler, *Sulfate Attack on Concrete*, Spon Press, New York, 2002.
- [4] P.J.M. Monteiro, K.E. Kurtis, Time to failure for concrete exposed to severe sulfate attack, *Cem. Concr. Res.* 33 (7) (2003) 987–993.
- [5] M. Santhanam, M.D. Cohen, J. Olek, Sulfate attack research—whither now?, *Cem. Concr. Res.* 31 (6) (2001) 845–851.
- [6] W.G. Hime, B. Mather, Sulfate attack or is it? *Cem. Concr. Res.* 29 (5) (1999) 789–791.
- [7] A. Xu, A. Shayan, P. Baburamani, Test methods for sulfate resistance of concrete and mechanism of sulfate attack, *Review Report - ARRB Transport Research* 5 (1998).
- [8] M.D. Cohen, B. Mather, Sulfate attack on concrete—research needs, *ACI Mater. J.* 88 (1) (1991) 62–69.
- [9] ASTM, Standard test method for length change of hydraulic-cement mortars exposed to a sulfate solution, *ASTM Standard C1012 - 95a*, Annual Book of ASTM Standards, 1996.
- [10] P.K. Mehta, Evaluation of sulfate-resisting cements by a new test method, *ACI J.* 72 (1975) 573–575.
- [11] K.E. Kurtis, K. Shomglin, P.J.M. Monteiro, J. Harvey, J. Roesler, Accelerated tests for measuring resistance of calcium sulfoaluminate, calcium aluminate, and Portland cements, *ASCE, J. Mater. Civ. Eng.* 13 (3) (2001) 216–221.
- [12] American Concrete Institute (ACI), 201.2R-92: *Guide to Durable Concrete*, Farmington Hills, Michigan, 1992.
- [13] American Concrete Institute (ACI), 201.2R-01: *Guide to Durable Concrete*, Farmington Hills, Michigan, 2001.
- [14] S.R. Stock, N.N. Naik, A.P. Wilkinson, K.E. Kurtis, X-ray microtomography (microCT) of the progression of sulfate attack of cement paste, *Cem. Concr. Res.* 32 (10) (2002) 1673–1675; Errata 32 (12) (2002) 2002.
- [15] N. Naik, K. Kurtis, A. Wilkinson, A. Jupe, S. Stock, Sulfate deterioration of cement-based materials examined by X-ray microtomography, *Proc. SPIE 49th Annual Meeting, Optical Science and Technology: Developments in X-ray Tomography: IV*. Denver, August 2–6, 2004.
- [16] A.C. Jupe, S.R. Stock, P.L. Lee, N. Naik, K.E. Kurtis, A.P. Wilkinson, Phase composition depth profiles using spatially resolved EDXRD, *J. Appl. Crystallogr.* 37 (2004) 967–976.
- [17] I. Odler, I. Jawed, Expansive reactions in concrete, in: J. Skalny, S. Mindess (Eds.), *Materials Science of Concrete: II*. American Ceramic Society, 1991, pp. 221–247.
- [18] P.K. Mehta, personal communication with N.N. Naik.

- [19] Rasheeduzzafar, Influence of cement composition on concrete durability, *ACI Mater. J.* 89 (6) (1992) 574–586.
- [20] P.W. Brown, An evaluation of the sulfate resistance of cements in a controlled environment, sulfate resistance of concrete, George Verbeck Symposium, ACI SP-77, 1982, pp. 83–91.
- [21] R.S. Gollop, R.S., H.F.W. Taylor, Microstructural and microanalytical studies of sulfate attack. I. Ordinary Portland cement paste, *Cem. Concr. Res.* 22 (6) (1992) 1027–1038.
- [22] R.S. Gollop, R.S., H.F.W. Taylor, Microstructural and microanalytical studies of sulfate attack: II. Sulfate-resisting Portland cement: ferrite composition and hydration chemistry, *Cem. Concr. Res.* 24 (7) (1994) 1347–1358.
- [23] R.S. Gollop, R.S., H.F.W. Taylor, Microstructural and microanalytical studies of sulfate attack: III. Sulfate-resisting Portland cement: reaction with sodium and magnesium sulfate solutions, *Cem. Concr. Res.* 25 (7) (1995) 1581–1590.
- [24] Rasheeduzzafar, O.S.B. Al-Amoudi, S.N. Abduljawwad, M. Maslehuddin, Magnesium–sodium sulfate attack in plain and blended cements, *ASCE, J. Mater. Civ. Eng.* 6 (2) (1994) 201–222.
- [25] N.N. Naik, Sulfate attack on Portland cement-based materials: Mechanisms of damage and long-term performance, PhD thesis, Georgia Institute of Technology, Atlanta, Georgia, 2003.
- [26] O.S.B. Al-Amoudi, Performance of fifteen reinforced concretes in magnesium–sodium sulphate environments, *Constr. Build. Mater.* 9 (1) (1995) 25–33.
- [27] H. Haynes, Sulfate attack on concrete: laboratory vs. field experience, *Concr. Int.* 24 (7) (2002) 64–70.
- [28] C.J. Hampson, J.E. Bailey, The microstructure of the hydration products of tri-calcium aluminate in the presence of gypsum, *J. Mater. Sci.* 18 (1983) 402–410.
- [29] P.K. Mehta, P.J.M. Monteiro, *Concrete: Microstructure, Properties, and Materials*, 2nd edition, Prentice-Hall, Englewood Cliffs, NJ, 1993.
- [30] G.W. Scherer, Crystallization in pores, *Cem. Concr. Res.* 29 (8) (1999) 1347–1358.
- [31] M.A. Gonzalez, E.F. Irassar, Ettringite formation in low C3A Portland cement exposed to sodium sulfate solution, *Cem. Concr. Res.* 27 (7) (1997) 1061–1072.